Nuclear Instruments and Methods in Physics Research A 1062 (2024) 169191

Contents lists available at ScienceDirect

Nuclear Inst. and Methods in Physics Research, A

journal homepage: www.elsevier.com/locate/nima

Full Length Article

Enrichment measurement by passive γ-ray spectrometry of uranium dioxide fuel pellets using a europium-doped, strontium iodide scintillator

Andrew J. Parker [a,*], Manuel Bandala [a], Stephen Croft [a], Laurie Crouch [c], R. David Dunphy [b], Daniel Hutchinson [d], Roy Logsdon [c], Xiandong Ma [a], Stephen Marshall [b], Paul Murray [b], Ali Sarfraz [c], Paul Stirzaker [d], James Taylor [a], Jaime Zabalza [b], Malcolm J. Joyce [a]

[a] School of Engineering, Lancaster University, Bailrigg, Lancaster, LA1 4YR, UK
[b] Department of Electronic and Electrical Engineering, University of Strathclyde, Glasgow, G1 1XW, UK
[c] National Nuclear Laboratory, Springfields, Salwick, Preston, PR4 0XJ, UK
[d] Westinghouse Springfields Fuels Ltd., Springfields, Salwick, Preston, PR4 0XJ, UK

ARTICLE INFO

Keywords:
Enrichment meter principle
Passive γ-ray analysis
Strontium iodide
Infinite thickness

ABSTRACT

The performance of a europium-doped strontium iodide scintillator for uranium enrichment measurement of a variety of sintered uranium dioxide fuel pellets is described and compared to that of caesium iodide and sodium iodide. Enrichment has been determined via passive γ-ray spectrometry of the 186 keV line from uranium-235 using gross count, net count, and peak ratio analyses. The 38 mm Ø x 38 mm strontium iodide crystal demonstrates superior energy resolution (3.43 ± 0.03% at 662 keV) and competitive detection efficiency for its size in the energy range of interest for uranium enrichment analysis (<250 keV). It demonstrates better χ^2_ν and coefficient of determination values than caesium iodide and sodium iodide when measuring uranium enrichment using the gross- and net-count from the 186 keV emission. It is shown to have the least measurement variance of the three scintillators studied in determining the uranium enrichment of pellets in a blind test, with a relative error comparative to sodium iodide and smaller than caesium iodide. This research heralds the potential of strontium iodide in passive γ-ray uranium enrichment applications.

1. Introduction

The need to determine ^{235}U enrichment in uranium-containing materials is of fundamental importance in the nuclear industry. Several different analytical techniques exist that can provide accurate and precise isotopic ratio data of uranium materials. These fall into two categories concerning mass spectrometry and γ-ray spectroscopy.

Mass spectroscopy techniques include: thermal ionisation mass spectroscopy, inductively coupled plasma mass spectroscopy (ICP-MS), and laser ablation ICP-MS, amongst others. These techniques provide accurate and precise isotopic quantification with small measurement uncertainties. However, the cost, technical complexity, and sample preparation times are significant disadvantages that can limit the adoption of these techniques. This is particularly the case when isotopic information is required frequently and in near real-time to render manufacturing processes responsive to any deviation from specified enrichments [1].

γ-ray spectroscopy offers a more economical approach, both in terms of cost and time. It can be applied to spontaneous or induced γ-ray emissions from relevant nuclides in uranium-containing materials to quantify the isotopic composition [2]. However, γ-ray spectroscopy has measurement capabilities that are typically an order of magnitude less sensitive than mass spectrometry analyses [1].

The measurement of ^{235}U enrichment in bulk solid samples of uranium has long been achieved passively via γ-ray spectroscopy, based on the 185.72 keV γ-ray emission (rounded to as 186 keV for the remainder of this work for brevity) that occurs in 57.1% of ^{235}U decays is characteristic the isotope and is relatively clear of contaminant lines from neighbouring isotopes. From the magnitude of the 186 keV γ-ray photopeak, the proportion of ^{235}U can be estimated using one of several spectroscopic methods. A well-established example is the *infinite thickness technique*, where a uranium sample is viewed with a γ-ray detector through a collimated channel [3]. Due to its high atomic number and density, uranium or uranic compounds attenuate their own γ-ray

* Corresponding author.
E-mail address: a.j.parker3@lancaster.ac.uk (A.J. Parker).

https://doi.org/10.1016/j.nima.2024.169191
Received 3 October 2023; Received in revised form 31 January 2024; Accepted 16 February 2024
Available online 23 February 2024

emissions so that only a fraction of the radiations emitted from a sample reach the detector.

For sintered UO_2 fuel pellets the mean free path for 186 keV γ-rays is 0.7 mm [3]. Using the convention of seven mean free paths [4], UO_2 has an infinite thickness of 4.9 mm, therefore any 186 keV γ-rays emitted from a depth greater than 4.9 mm have a probability of ≤0.1% of traversing this distance without being attenuated or absorbed [3]. If the depth of the samples along the collimator axis is significantly greater than the mean free path of the 186 keV γ-rays, all samples of the identical physical composition would present equal visible volumes to the detector. Consequently, one of the core assumptions in the use of the *infinite thickness technique* is that the whole sample is isotopically homogeneous. The technique assumes any variation in the recorded 186 keV γ-ray emissions between two samples is due to a corresponding difference in the ^{235}U content from one sample to the other [3].

Alternatively, enrichment can be inferred from the ratio of the magnitude of the full-energy peaks associated with γ-ray emissions from different isotopes of uranium in a sample, such as the 186 keV and 1001 keV γ rays from ^{235}U and ^{238}U in a sample, respectively [3]. Peak *peak-ratio methods* have the advantages of having fewer experimental geometry considerations, plus the infinite thickness requirement does not need to be met. However, the ^{238}U in a sample must be in secular equilibrium with its daughter products for the technique to be applicable [3].

Inorganic scintillators, such as thallium-doped sodium iodide (NaI [Tl]) or caesium iodide (CsI[Tl]), are in widespread use for passive γ-ray analysis due to their low cost, high detection efficiency and satisfactory energy resolution. In this work we evaluate experimentally the europium-doped inorganic scintillator, strontium iodide $SrI_2(Eu)$ for uranium enrichment determination, as it has several attractive features compared to the established scintillation materials [5].

$SrI_2(Eu)$ was patented as a scintillation medium in 1968 [6]. In 2008, modifications were made to the route by which it is synthesised rendering it viable for more widespread scintillation applications, demonstrating excellent detection characteristics compared to more commonplace scintillation media [5]. A summary of the general material and scintillation attributes for $SrI_2(Eu)$ and other common scintillators is given in Table 1.

The data in Table 1 demonstrate why $SrI_2(Eu)$ might compete with long-established alternatives: It has a light yield double that of CsI(Tl) and $LaBr_3(Ce)$, and up to four times that of the scintillant in most widespread use, NaI(Tl). Consequently, it has a better energy resolution, evidenced by a lower full-width half maximum (FWHM) value and a relatively high density resulting in a higher stopping power for higher-energy photons. However, the manufacture of $SrI_2(Eu)$ crystal sizes greater than 103 cm^3 has not been reported, in part due to the self-absorption of its own scintillation light and it has a longer light response time [8–10]. These features increase the chances of pulse pile-up and dead time when analysing higher activity sources and decreases energy resolution [11]. Consequently, $SrI_2(Eu)$ may suffer in terms of detection efficiency compared to that of NaI(Tl) and, to a lesser extent, CsI(Tl), which can be manufactured in much larger or more geometrically complex volumes (>10,570 cm^3 for single NaI(Tl) crystals). In this research, the capability of $SrI_2(Eu)$ in the measurement of ^{235}U enrichment in UO_2 is reported, relative to NaI(Tl) and CsI(Tl) scintillators.

2. Materials and methods

2.1. Equipment and sources

Three different inorganic scintillators were used in this comparative study. Table 2 lists the types, parameters, and manufacturer information. The scintillation detectors were connected to a laptop personal computer via USB to a digital PMT-base connected to the scintillator photomultiplier tubes. Two PMT-bases were used in this work, a bMCA USB Multi-Channel Analyzer (BrightSpec NV/SA, Belgium) for the CsI (Tl) and $SrI_2(Eu)$ and a digiBASE (ORTEC®/AMETEK® Inc., USA) to control the NaI(Tl). The PMT-bases were connected to the scintillator photomultiplier tubes via the 14-Pin PMT and controlled using BrightSpec (BrightSpec NV/SA, Belgium) or MAESTRO (ORTEC®/AMETEK® Inc., USA) multichannel analyser simulator software.

For the calibration measurements and initial detection comparison study, point and volume sources were used, including the isotopes ^{60}Co, ^{137}Cs, ^{152}Eu, ^{226}Ra and ^{241}Am. Additionally, slices of depleted uranium dioxide (DUO_2) light water reactor fuel pellets were used as a calibration source for ^{235}U and ^{238}U and their respective decay products. For uranium enrichment analysis, advanced gas-cooled reactor (AGR) UO_2 fuel pellets were used, sufficiently aged for the ^{238}U to be in secular equilibrium, produced by the UK's National Nuclear Laboratory (Preston, UK). AGR pellets are cylindrical with dimensions of 14.500 mm Ø x 15.000 mm height, with a central annulus 6.350 Ø mm giving a wall thickness of 4.075 mm along the collimation-detector axis, 0.825 mm less than the theoretical infinite thickness of sintered UO_2 (4.900 mm) [12]. However, as the central annulus contains no material with significant attenuation capabilities, the 186 keV γ-rays emitted from within 0.825 mm of the far side of the annular cylinder can still reach the detector. As such, the pellet volume can be considered to meet the infinite thickness criteria.

The ^{235}U mass, and therefore the enrichment, in the pellets was measured by multi-collector, inductively-coupled plasma mass spectrometry (MC-ICP-MS) at Westinghouse's Springfields site (Preston, UK). All pellet enrichments referred to in this manuscript are expressed as the uranium enrichment by weight percentage (%wt or E_w) of the ^{235}U mass relative to the overall mass of uranium within the pellet.

The experimental setup for the calibration measurements and single pellet analysis is shown Fig. 1. The detectors were positioned perpendicular to the collimated source beam as this allows for better optimising energy resolution [9,13]. Cantilever laboratory jacks were used to ensure the centre of the collimator opening intersects halfway up the height of the detector sensitive volume. The sources and pellets were placed such that the centre of the source under analysis was positioned 57.5 mm from the detector surface. Between the source and detector was a 50 mm thick lead collimator with an 8 mm Ø opening. As shown in Fig. 1B, additional 50 mm lead chevrons were positioned around the detector to reduce the influence of background count.

2.2. Peak fitting and data analysis

Raw spectral collected from the detector setups were treated with a

Table 1
Summary of the material and scintillation characteristics of common inorganic scintillators [7,8].

Parameter	$SrI_2(Eu)$	NaI(Tl)	CsI(Tl)	$LaBr_3(Ce)$	BGO	LSO
Density (g cm^{-3})	4.6	3.4	4.5	5.3	7.1	7.4
Mean Free Path @ 186 keV (cm)	0.67	0.90	0.58	0.69	0.19	0.24
Light yield (photons MeV^{-1})	≤120,000	38,000	66,000	61,000	10,000	30,000
Decay time (ns)	600-2400	230	1100	35	300	40
Resolution (% @ 662 keV)	4	7	6	3	≥15	≥12
Wavelength of emission (nm)	430	410	540	360	480	420

Table 2
Manufacturer information, dimensions and technical specifications of the detectors used in this comparison study.

Detector crystal compound	Dimensions (mm)	Sensitive volume (cm^3)	Manufacturer	Detector Serial Number	Datasheet Resolution @ 662 keV	PMT
NaI(Tl)	75.2 Ø x 75.2	347.5	Ortec/Bicron	60005-03864-I	<7.5 %	Hamamatsu R1307
CsI(Tl)	50 × 50 x 50	125.0	Scionix	SER678	<10.0 %	Hamamatsu R3234
$SrI_2(Eu)$	38 Ø x 38	43.1	Scionix	S1AB1467	<3.5 %	Hamamatsu R6231

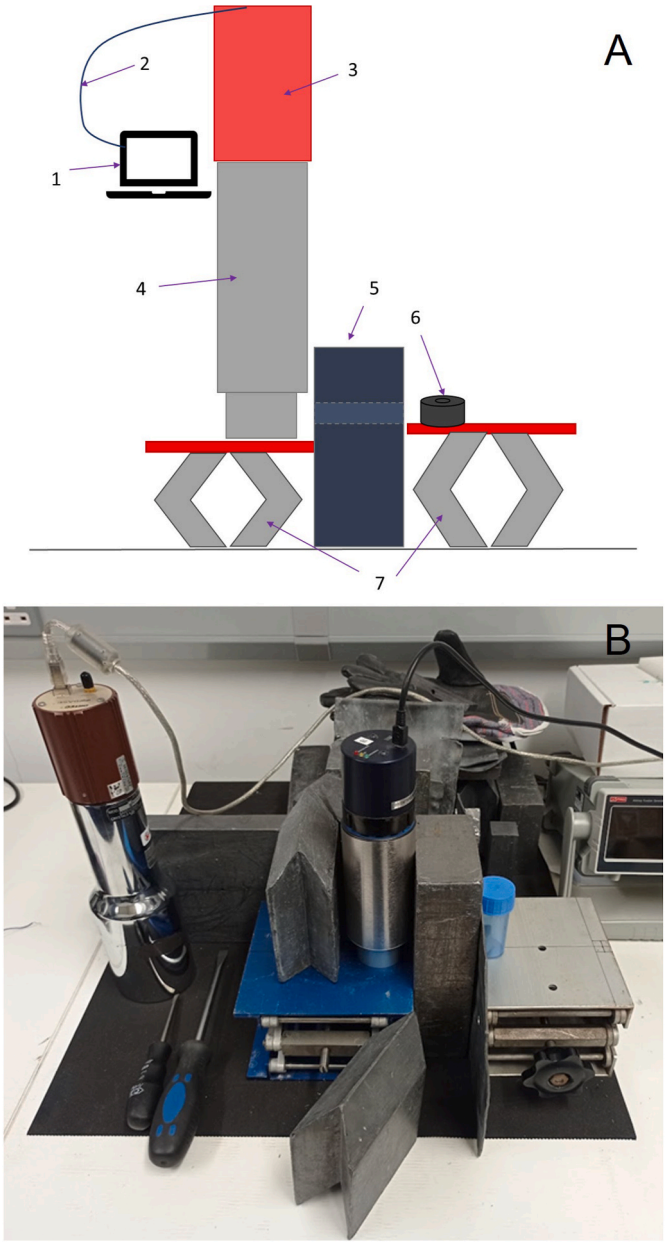

Fig. 1. A Side elevation schematic of the calibration source and single pellet experimental setup (not to scale) without lead chevrons surrounding the detector to enable clarity, where 1) PC, 2) USB cable, 3) digital PMT-base, 4) SrI2 (Eu) detector, 5) 50 mm thick lead collimator with 8 mm opening, 6) AGR pellet or calibration point-source, 7) Cantilever laboratory jacks. B) Photograph of the experimental setup using a $SrI_2(Eu)$ scintillator connected to a bMCA USB PMT-base, with an aluminosilicate simulated AGR pellet with a lead chevron removed to allow viewing of the detector. The NaI(Tl) used in this work is shown on the left of the photograph, connected to a DigiBASE PMT -base.

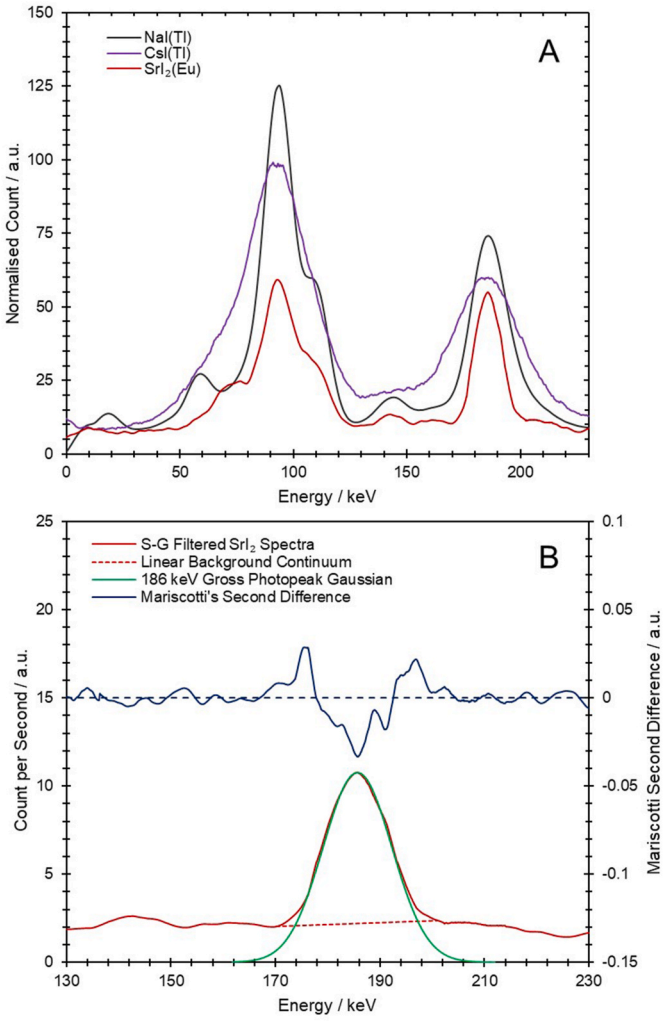

Fig. 2. A) Savitzky-Golay filtered γ-ray spectra of a 4.460 ± 0.005 %wt enriched AGR fuel pellet, collected from the NaI(Tl), CsI(Tl), and $SrI_2(Eu)$ scintillators in the 0–230 keV range using a 400 s live count time, B) 186 keV full-energy peak collected using the $SrI_2(Eu)$ detector, linear background continuum under the full-energy peak, Mariscotti's second difference plot used to identify peak limits, and gaussian distribution identifying the gross count full-energy peak.

shaping algorithm including a Savitzky-Golay filter using a 9-channel window and appropriate filter coefficients in Python (SciPy) [14]. Fig. 2A shows smoothed spectra up to 230 keV of a 4.460 %wt enriched AGR fuel pellet from the three scintillation detectors used. Full-energy peak channel widths were determined using Mariscotti's second difference method also shown in Fig. 2B [15]. The gross counts from the full-energy peak were calculated from the sum of the counts from the channels within the specified peak area. The net count from a full-energy peak was calculated by subtracting a background continuum count from the gross count. Fig. 2B shows the background continuum between two values calculated from the average of seven channels either side of the full-energy limits. As can be seen in Fig. 2B, the background continuum was assumed to be a linear regression under the full-energy peak bounds.

As seen in Fig. 2B, the ^{235}U γ-ray 163.4 and 205.3 keV (both 5.1 %

emission probability [16]) full-energy peaks are evident as small bumps either side of the 186 keV full-energy peak collected with the $SrI_2(Eu)$. The weak 202.1 keV emission (1.1 % emission probability [16]) from ^{235}U is subsumed by the tail of the 186 keV full-energy peak, where the small tail is a residue of the light trapping within the crystal volume, caused by the low emission probability and an overlap in the absorbance and radioluminescence of the europium dopant that increases the effective light decay time [17–19]. The 163.4 and 205.3 keV full-energy peaks are not visible in the NaI(Tl) and CsI(Tl) spectra, due to the poorer energy resolution. The NaI(Tl) is able to identify the 143.8 keV full-energy peak clearly and this energy region is also evident in the CsI (Tl) spectra but the full-energy peak is not evident and included within the background count in that energy region.

Given the inability of the NaI(Tl) and CsI(Tl) to resolve the 163.4 and 205.3 keV full-energy peaks, these emissions were partly included in the full-energy peak counts for these detectors, complicating the analysis of the 186 keV peak in isolation. When discussing the 186 keV full-energy peak for the NaI(Tl) and CSI(Tl) detectors for the remainder of this manuscript it will include the 163.4, 202.1, and 205.3 keV ^{235}U emissions unless explicitly stated.

For the net count, a background contribution was subtracted from the gross count, and this was determined assuming a linear background continuum beneath the 186 keV full-energy peak. The start and end points for this background continuum were taken from the average of seven channels either side of the full-energy peak with a linear fit then calculated between these two values. To calculate the peak ratio (P_R), the gross count levels of both the 186 keV (C_{186}) and 1001 keV (C_{1001}) full-energy peaks were determined for the ^{235}U and ^{238}U isotopes, respectively, and determined using (1).

$$P_R = \frac{C_{1001}}{C_{186}} \tag{1}$$

3. Results and discussion

3.1. Detector performance comparison

The energy resolutions for the three scintillators studied are shown in Fig. 3, derived from the Full Width Half Maximum (FWHM) of full-energy peaks between 59.5 and 1332 keV. Given the different light response and decay times of the scintillators used in this study [13,20,21], the optimal resolution values for the calibration study were achieved by adjusting the detectors high voltage, fine gain, and pulse shaping filter parameters for each calibration source and γ-ray emission studied, these parameters are shown in Table 3.

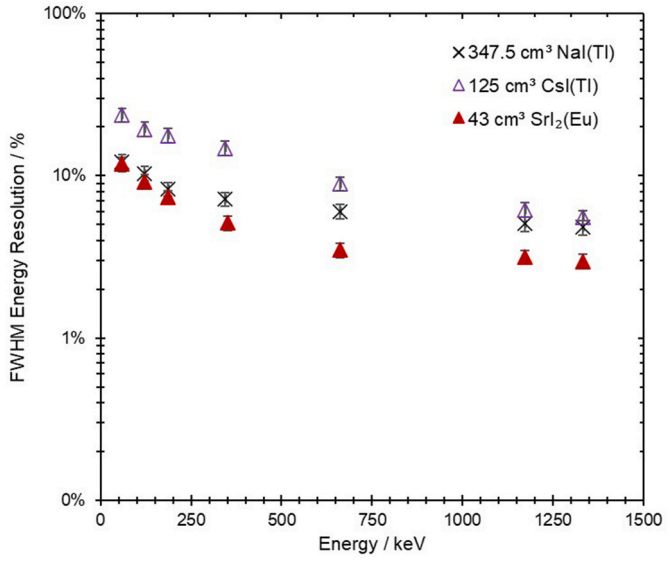

Fig. 3. Energy resolution of the NaI(Tl), CsI(Tl), and $SrI_2(Eu)$ as a function of the γ-ray energies emitted from a selection of radioactive calibration sources.

Evidently, the $SrI_2(Eu)$ has the best FWHM resolution, with the NaI (Tl) and CsI(Tl) scintillators following the expected energy resolution performance reported elsewhere in the literature [22]. The resolution for $SrI_2(Eu)$, 3.43 ± 0.03% at 662 keV, is well within the range of FWHM resolution values for the material, reported typically between 2.93 and 4.00%, and within the instruments certificated performance, i.e. <3.5 % at 662 keV [23]. The overall resolution may be further optimised through minute adjustments to the experimental geometry, collimation, and background attenuation. As an example, Takabe et al. (2016) demonstrated a variation in resolution in $SrI_2(Eu)$ (between 3.29 ± 0.02 % and 4.13 ± 0.02 % at 662 keV) due to the location of a collimated γ-ray beam from a ^{137}Cs source relative to the sensitive volume and photocathode [13]. Similarly, Sturm et al. (2010) showed a change in energy resolution at 662 keV from 5.0 % to 3.2% for a 19.7 cm^3 $SrI_2(Eu)$ cylindrical crystal by moving the interaction point in the sensitive volume away from the photocathode [9]. These geometrical considerations also contribute to reducing the size of the full-energy peak tail. Further reduction of the $SrI_2(Eu)$ full-energy peak tail, caused by light trapping, can be accomplished through digital pulse processing optimisation [17]. This would not affect the FWHM value primarily as the tail appears beneath the half-maximum measurement value, but it would improve the full width at one-fifth maximum and could allow identification of the 202.1 keV emission with long enough counting times.

Compared to literature, Hawrami et al. (2020) reported a resolution of 2.9% (@ 662 keV) for europium-doped thallium strontium iodide ($TlSr_2I_5[Eu]$), a similar but different chemical composition, with a volume 1.39 cm^3 [24], which is more than 0.4 % better than for the $SrI_2(Eu)$ used here. The best-reported resolution for $SrI_2(Eu)$ appears to be 2.93% by Sturm et al. (2010) for a 13 cm^3 tapered cylindrical crystal doped with 3% europium. Using a silicon photomultiplier (SiPM) attached to a 2 cm^3 $SrI_2(Eu)$ crystal, Mitchell and Philips (2016) recorded a 3.8% resolution at 662 keV consistent with other works but with the marginally poorer resolution associated with SiPMs [25]. They also noted nonlinearity in the energy calibration, consistent with the use of SiPMs [26]. Without correcting for the nonlinearity, the FWHM was recorded as 2.6% [27]. Likewise, Takabe et al. (2016) achieved a resolution of 3.29% at 662 keV for a comparatively large $SrI_2(Eu)$ scintillator (>10 cm^3) [13]. In addition to this finding, the authors compared 12 cm^3 and 25 cm^3 crystals and noted a decrease in energy resolution for the larger crystal size. The poorer resolution of larger $SrI_2(Eu)$ crystals was also reported by Giaz et al. (2015), reporting a FWHM of 4.0% (@ 662 keV) for a 103 cm^3 $SrI_2(Eu)$, one of the largest reported [20]. Finally, Raja et al. (2018) reported comparatively poor energy resolution performance of 4.6%, 7.5% and 9.8% for 662 keV, 122 keV, and 1332 keV emissions, respectively, for single $SrI_2(Eu)$ crystals (estimated volume <9 cm^3) grown using the Bridgman technique [28]. The authors state the results may be affected by crystal inhomogeneity and oxygen contamination. Given the hygroscopic nature of $SrI_2(Eu)$, exposure to air can cause significant reduction in its optical parameters [28].

The variation in $SrI_2(Eu)$ energy resolution performance over increasing crystal volumes contrasts with convention for other scintillators, such as NaI(Tl). Typically, larger scintillation crystals have better

Table 3
High voltage range and pulse shaping filter parameters used for the calibration study.

Detector	High Voltage Range (V)	Rise Time (μs)	Flat Top Time (μs)	Pole-to-Zero (μs)	FWHM @662 keV	FWHM @186 keV
$SrI_2(Eu)$	650–780	12.0	4.0	2.0	3.43%	7.39%
NaI(Tl)	800–1000	0.8	0.2	2.0	6.22%	8.25%
CsI(Tl)	890–1100	4.0	2.0	2.0	8.96%	17.76%

energy resolution due to larger volumes increasing the likelihood of total absorption of the γ-ray photons, rather than scattering out of a given detector volume [11,29]. The results of this work and those reported in the above studies provide evidence to the conclusions reached by Alekhin et al. (2010), that an increase in volume of a $SrI_2(Eu)$ crystal correlates strongly with a decrease in overall light-yield and increase in the likelihood of scintillation photon re-absorption [10,13,30]. Other factors, such as temperature and electrical noise also effect resolution, but given the measurement conditions and equipment were consistent between experiments, it is not anticipated that these aspects will have a significant bearing on the above results [31].

In addition to energy resolution, detection efficiency is also influenced by the choice of scintillator material, its volume and shape, and density, with higher efficiencies associated with denser (higher-Z) materials [24]. From Tables 1 and it can be seen that CsI(Tl) has the shortest mean free path for 186 keV γ-ray (0.75 cm) of the detectors used in this research. The most dense material $SrI_2(Eu)$ having the next shortest and NaI(Tl), the least dense, the farthest at 0.67 and 0.90 cm, respectively. A shorter mean free path equates to a higher probability that the γ-ray will interact with the material and will therefore be detected, implying a higher detection efficiency. These factors contribute to the total material cross sections. Fig. 4 shows the total linear attenuation cross sections, including Compton scattering, for the three scintillation materials used here, generated using XCOM Photon Cross Sections Database and normalised for the respective material densities [32].

As shown in Fig. 4, all three scintillators have similar linear attenuation coefficient values in the energy range under consideration (10–1100 keV), and therefore similar material detection efficiencies. For energies <40 keV the $SrI_2(Eu)$ has the higher attenuation and therefore a higher potential material efficiency. For 186 keV photons of interest in this study, $SrI_2(Eu)$ displays a total linear attenuation coefficient of 0.085 cm^{-1}, with CsI(Tl) and NaI(Tl) having cross sections of 0.107 and 0.124 $cm^2\ g^{-1}$, respectively.

The $SrI_2(Eu)$ is the only detector used here where the distance of seven mean free paths for the 186 keV γ-ray is greater than the depth of the scintillator crystal along the pellet-collimator axis. Therefore, it would be expected that some of the 186 keV photons to pass through the $SrI_2(Eu)$ detector volume without interacting, lowering the overall absolute efficiency of the detector used in this work.

The comparatively long light decay time of $SrI_2(Eu)$ also affects the absolute efficiency. As shown in Table 2, $SrI_2(Eu)$ requires a shaping time 2–12 times greater than other scintillators used here. Using longer shaping times can increase the proportion of dead time, the time that pulses from incident γ-ray photons cannot be recorded whilst the circuitry is processing a previous interaction [8,11]. Consequently, this can reduce the efficiency of the detector, particularly in high-count environments. Given the relatively low radioactivity of the point sources used here, 0.04–0.4 MBq, and the collimated experimental geometry, the recorded detector dead time difference between the detectors was 0.03–1.74% for the NaI(Tl) and 0.35–9.20% for the $SrI_2(Eu)$ across the source activity range.

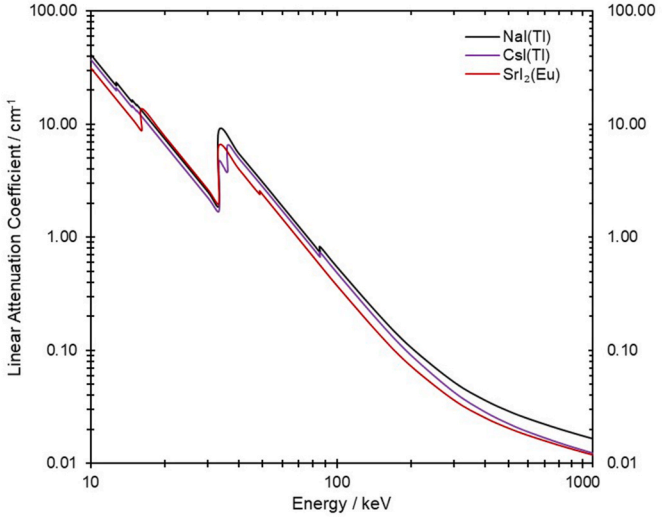

Fig. 4. NIST-COM generated linear attenuation coefficients for the NaI(Tl), CsI (Tl), and $SrI_2(Eu)$ scintillators as a function of the photon energy in the range 10–1100 keV.

The results of this comparison of energy resolution study and detection efficiency discussion illustrates the benefits of $SrI_2(Eu)$. When considering the requirements for energy resolution, the $SrI_2(Eu)$ is shown to be superior to NaI(Tl) and CsI(Tl) at γ-ray energies between 60 and 1332 keV and particularly at 186 keV, the photon energy of interest for uranium enrichment measurements based on infinite thickness technique [3]. Across the energy range, the $SrI_2(Eu)$ outperforms the other scintillators in terms of resolution and is comparable with regards to efficiency, indicating suitability for use in mixed isotopic environments where individual sources require differentiating and quantifying.

3.2. Single pellet uranium enrichment measurements

A variety of individual AGR fuel pellets was assessed using the three scintillators described above, with each of the pellets placed 57.5 mm from the detector casing, as shown in Fig. 1, and counted for a period of 400 s. A list of the pellet enrichments by their weight percentage of ^{235}U is given in Table 4. No containers or shielding were used between the pellets and detector, and the pellets were not observed to contain contaminants that need to be considered, given shielding or contamination can affect the measurement [33–36].

As the experimental geometry meets the infinite thickness criteria, the mass of ^{235}U in the pellets will be proportional to the magnitude of the count taken from the 186 keV full-energy peak [3,37]. This is what is shown for both the gross and net counts in Figs. 5 and 6. For all three datasets, as the ^{235}U mass in the AGR pellet increases with increasing enrichment, the gross and net counts are observed to increase proportionally. The relationships between the enrichment and full-energy peak count (gross and net count) were determined using the count data, associated errors and the least-squares method, and characterised using the reduced chi-squared (χ^2_ν) methodology, where ν are the degrees of freedom ($\nu = 6$) [38]. The results of the χ^2_ν tests are given in the insets of the Figures.

For the gross count method, the $SrI_2(Eu)$ data set appears the most linear as it displays the χ^2_ν value closest to unity, 0.955, compared to 0.931 and 5.815 for NaI(Tl) and CsI(Tl), respectively. However, the NaI (Tl) has the best fit when comparing r^2 value, the 0.990, slightly better than that of $SrI_2(Eu)$. The CsI(Tl) data yield the least best fit, which is apparent from Fig. 5. Given the variation in the data points and the distance from the predicted linear model data points, particularly for the 1.248 and 1.952 %wt pellets, it could be considered that the pellets are of a different enrichment than stated. This is unlikely to be due to a real distinction in enrichment given the pellets have been characterised independently by the UK's National Nuclear Laboratory with an enrichment absolute measurement error of ±0.005% E_w. As such, the likely cause is suspected to be a slight alteration in placement of the pellet or detector when positioned for analysis, manifest as slight changes in count-rate due to changes in distance from the detector as per the inverse-square dependence. This anomaly could also be rectified by using longer counting durations to lessen the impact of any random statistical variation. Smaller anomalies are present for the 3.009 %wt pellet recorded with the $SrI^2(Eu)$ detector and the 1.763 and 1.952 %wt pellets recorded with the NaI(Tl) with likely the same root cause.

The net count values for the pellets measured show an increase in error compared to the gross count datasets. This is due to the propagation of error resulting from the net count being calculated from sub-

Table 4
The enrichments by weight % of the AGR UO_2 pellets used in the enrichment analysis in this work. Pellet enrichment absolute measurement error ±0.005 %wt supplied by NNL.

	AGR pellets used							
^{235}U content/%wt	1.248	1.763	1.952	2.496	2.624	3.099	3.520	4.460
^{235}U mass/g	0.26	0.37	0.41	0.53	0.56	0.66	0.75	0.95

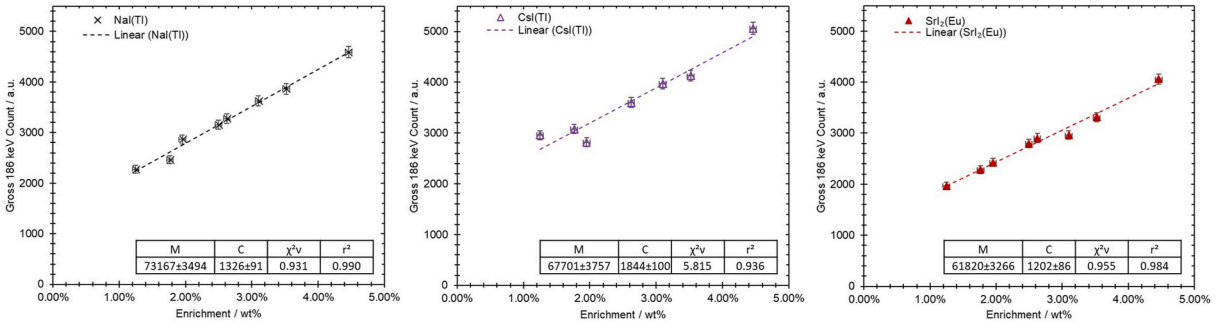

Fig. 5. Gross count for the 186 keV line of ^{235}U as a function of AGR pellet uranium enrichment by weight (wt%) for NaI(Tl), CsI(Tl) and SrI_2(Eu) detectors. Linear fits are included obtained using a weighted, least-squares minimisation with data for the gradient (M), intercept (C), χ_v^2 and r^2 included. All detectors employed a 400-s live time count. The error bars represent 1.65 standard deviation (~90% confidence interval).

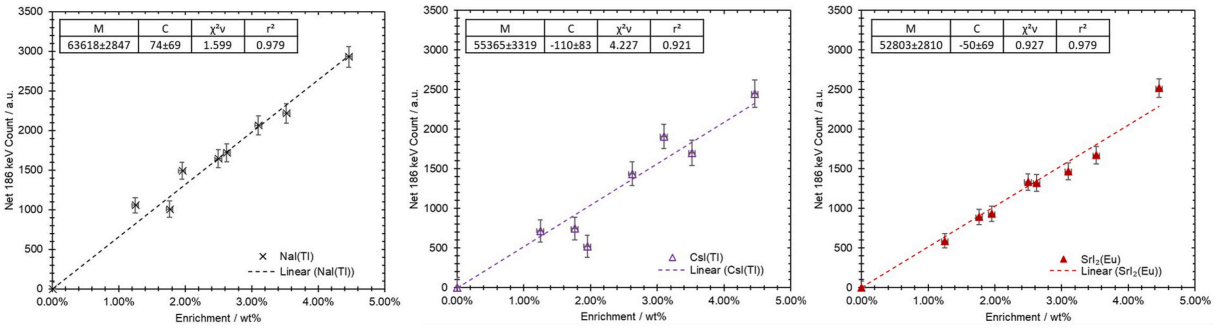

Fig. 6. Net count for the 186 keV line of ^{235}U as a function of AGR pellet uranium enrichment by weight (wt%) for NaI(Tl), CsI(Tl) and SrI_2(Eu) detectors. Linear fits are included obtained using a weighted, least-squares minimisation with data for the gradient (M), intercept (C), χ_v^2 and r^2 included. All detectors employed a 400-s live time count. The error bars represent 1.65 standard deviation (~90% confidence interval).

tracting a background count from the gross count. The linear regression fit for the net count dataset from the CsI(Tl) demonstrate an improvement in χ_v^2 when compared to the gross count model. The CsI(Tl) fit improved from 5.815 to 4.227. The SrI_2(Eu) regression fits appear to decrease marginally for the net count, going from a χ_v^2 of 0.950 for the gross-count model to 0.927 for the net count model, likewise for the NaI (Tl), 0.931 to 1.599 The r^2 for all datasets remain well over 0.9 therefore, despite the possible anomalies and over-fitting, the linear regressions reproduce the direct proportionality of the 186 keV full-energy peak count with ^{235}U percentage consistently.

The net count datasets for the NaI(Tl) and CsI(Tl) scintillators in Fig. 6 both show a greater variance with regard to the linear regression than gross count results, exaggerating the positioning inconsistencies discussed. This could be because of a greater variation in the measured background due to their poorer energy resolution including counts from the 163.4 and 205.3 keV emissions. Nevertheless, the data still follow the expected linear trend.

Comparing the values and model parameters in Figs. 5 and 6, the ratio of the net count and gross count can be determined, i.e., the ratio of ^{235}U 186 keV γ-rays to the underlying background or scattered photons in the full-energy peak energy range. The net-to-gross ratio is similar between the NaI(Tl) and the SrI_2(Eu). As an example, the gross and net counts rates recorded for 186 keV full-energy peak from 4.460 %wt pellet using the with the NaI(Tl) was 11.5 gross- and 7.3 net-counts per second, giving a net-to-gross ratio of 63.9 %. This compares to 10.1 and 6.3 counts-per-second for the gross and net count rates, respectively, using the SrI_2(Eu), giving a net-to-gross ratio of 62.1%. The CsI(Tl) had the worse net-to-gross ratio of 48.4% for the same pellet.

As stated above, the SrI_2(Eu) is at a disadvantage as a higher proportion of the 186 keV photons are likely to pass through the detector volume without interacting, compared to the larger NaI(Tl) and CsI(Tl) detectors, but is less susceptible to scattered photons. The larger volume NaI(Tl) and CsI(Tl) detectors are more likely to be in the path of photons that have scattered off the collimator or elsewhere, increasing background count noise.

In addition, the slightly increased proportion of detector dead time, caused by the longer pulse shaping times, could decrease the absolute efficiency and therefore the overall count. The percentage deadtime whilst assaying the highest activity pellet (4.460 %wt) with the SrI_2(Eu) was 0.76%, equivalent to 3.05 s or approximately 30.3 full-energy peak gross counts over a 400 s *real time* count. Given the experiments were run using *live time* count mode, any effects of increasing dead-time were mitigated, though this does have implications for the limits of detection study in Section 3.4.

The better net-to-gross count ratio will contribute to smaller relative error in the SrI_2(Eu) net-count values over the gross-count values because of error propagation in the subtraction of the background count

[38]. Further, the net-to-gross count ratio for the NaI(Tl) and CsI(Tl) is made worse because of its poorer energy resolution resulting in the inclusion of a proportion of photons associated with the 163.3 and 205.1 keV emissions inflating the gross count. This is avoided for the $SrI_2(Eu)$ as its superior energy resolution allows for clear discrimination of these full-energy peaks and 186 keV line, which could potentially contribute to shorter assay times.

As per the earlier discussion, the peak-ratio method of enrichment measurement compares the magnitudes of the 186 keV and 1001 keV day from ^{235}U and ^{238}U, respectively. This has the advantage that the 186 keV and 1001 keV peaks are visible with scintillators of relatively low energy resolution, unlike the X-rays in the 80–100 keV range which can also be used for peak analysis [39,40]. However, a disadvantage is that the detection efficiency of the scintillators at these contrasting energies varies, complicating the analysis. Here, the absolute gross count values from the 186 and 1001 keV full-energy peaks were used. Unlike the net- and gross-count relationships with enrichment, the dependence of the ratio of the two full-energy peak intensities and uranium enrichment is not linear because the proportion of ^{238}U is changing only very slightly, Consequently, the magnitude of 1001 keV full-energy peak remains relatively static compared to the 186 keV full-energy peak, as per Fig. 7.

The χ_ν^2 values for the regression models applied to the peak ratio datasets are broadly consistent to those for the other datasets, with the largest change being the far poorer fit of the NaI(Tl), with a χ_ν^2 of 7.037 and an r^2 of 0.818, the worst of all the fitting values across the scintillators and measurement techniques. This is likely a result of propagation of counting inconsistencies, discussed above, in both the 186 and 1001 counts [38]. Otherwise, they exhibit a consistent fit for the other two detectors with the CsI(Tl) recording the best fit with a χ_ν^2 of 1.384. This is a result of a the larger crystal size of the CsI(Tl) compared to the SrI(Eu) increasing the chances of 1001 keV photons interacting in the sensitive volume. Though, like the gross- and net-count analysis, the inflation in the efficiency of the CsI(Tl) data may also evident here. The data and the linear regressions models here serve as calibration measurements for the analysis and determination of ^{235}U content of pellets with an unknown enrichment.

3.3. Blind tests of single pellets

A series of measurements were taken from a pellet of unknown enrichment that was selected at random from the pellet inventory listed in Table 4 and tested under blind conditions for a period of 150 s. The enrichment by weight of the pellet was calculated from the linear relationships and the associated error determined for the three enrichment measurement techniques (gross count, net count and peak ratio). The results from these measurements and the errors for each of the three methods are provided in Fig. 8, normalised for enrichment, with the data given in Table 5.

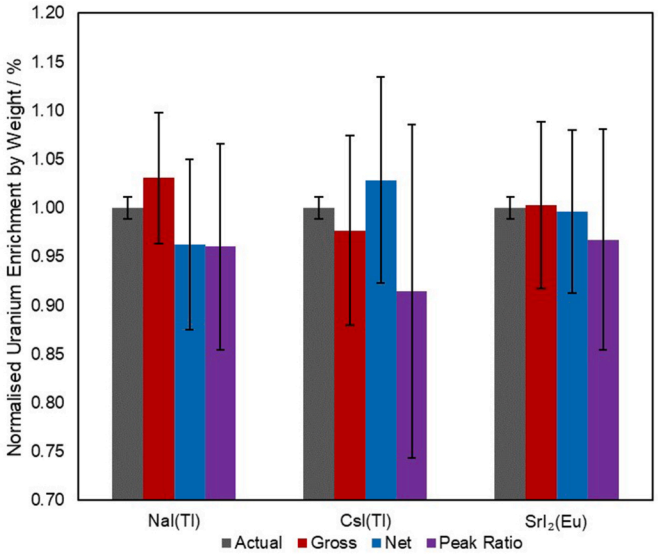

Fig. 8. Uranium enrichment by weight % measurements normalised to the value obtained by independent means of AGR fuel pellet chosen at random, measured with NaI(Tl), CsI(Tl), and $SrI_2(Eu)$ scintillators using the gross count, net count and peak ratio enrichment measurement methods. Error bars represent 95% CI or 1.96σ.

Table 5
Uranium enrichment by weight % measurements for the AGR fuel pellet (NNL) chosen at random as plotted in Fig. 4, and enrichments calculated using the gross count-rate, net count-rate and peak ratio enrichment measurements for the NaI (Tl), CsI(Tl), and $SrI_2(Eu)$. Actual enrichment values were verified using MC-ICP-MS. Stated errors for the measured results represent 95% CI or 1.96σ.

Detector	Actual ^{235}U enrichment (E_w)/%	Gross count ^{235}U enrichment (E_w)/%	Net count ^{235}U enrichment (E_w)/%	1001/186 keV peak ratio ^{235}U enrichment (E_w)/%
NaI(Tl)	(4.460 ± 0.005)%	(4.6 ± 0.3)%	(4.3 ± 0.4)%	(4.3 ± 0.5)%
CsI(Tl)	(4.460 ± 0.005)%	(4.4 ± 0.4)%	(4.6 ± 0.5)%	(4.1 ± 0.8)%
$SrI_2(Eu)$	(4.460 ± 0.005)%	(4.5 ± 0.4)%	(4.4 ± 0.4)%	(4.4 ± 0.6)%

For the blind test, the actual value for the pellet enrichment (4.460 % wt) falls within the values and error margins predicted by the three measurement methods and detectors used. From the results in Table 5, the $SrI_2(Eu)$ detector appears to have the smallest variance for the calculated enrichment value across the three methods used. However, the error values recorded for all detectors used are an order of

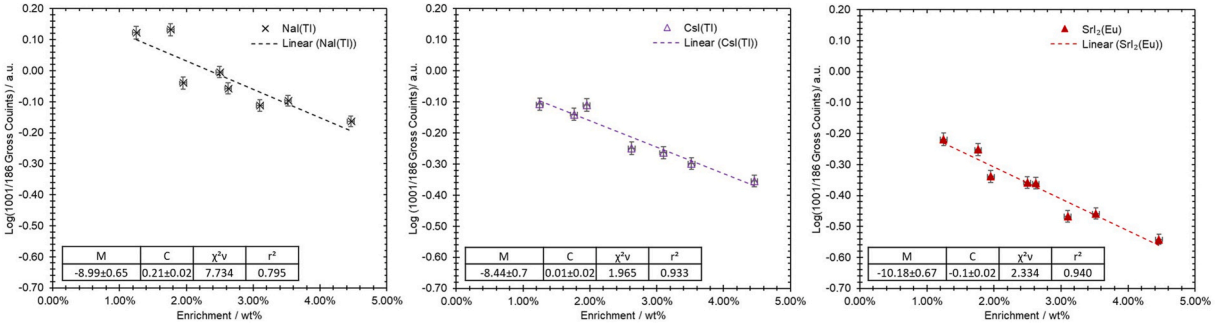

Fig. 7. Log_{10} of the 1001 keV/186 keV full-energy peak ratio as a function of AGR pellet uranium enrichment by weight (wt%) for NaI(Tl), CsI(Tl) and SrI2(Eu) detectors Linear fits are included obtained using a weighted, least-squares minimisation with data for the gradient (M), intercept (C), χ_ν^2 and r^2 included. All detectors employed a 400-s live time count. The error bars represent 1.96 standard deviation (~90% confidence interval).

magnitude greater than that used commonly in the manufacture of nuclear fuel, ±0.05% [41]. Longer counting durations or improvements to the geometric efficiency would lower this error and make the enrichment measurement more precise, but these parameters are dependent on the practical context for the use of passive γ-ray measurement and the number of pellets analysed.

3.4. Limits of detection

To establish the performance of the detectors in distinguishing between UO_2 pellets of similar but different enrichment, a limit of detection analysis was performed. This was done using the linear regression models determined from the experimental analysis in 3.2. The models were used to calculate the *real time* taken to differentiate between two pellets having enrichment by weights of 3.82 %wt and 4.00 %wt, as opposed to the *live time* used for the experiments above. For the analysis a Behrens-Welch test was used, sometimes referred to as Student's t-test with unequal variances, utilising Satterthwaite's approximation for the degrees of freedom (*df*) [42–44]. The test statistic (*d*) and *df* were calculated as follows:

$$d = \frac{x_1 - x_2}{\sqrt{\left(\frac{s_1^2}{n_1} + \frac{s_2^2}{n_2}\right)}}$$

$$df = \frac{\left(\frac{s_1^2}{n_1} + \frac{s_2^2}{n_2}\right)^2}{\frac{\left(s_1^2/n_1\right)^2}{n_1 - 1} + \frac{\left(s_2^2/n_2\right)^2}{n_2 - 1}}$$

where x_1 and x_2 are the sample means, calculated as the net count per second over the duration in seconds of the analysis, n_1 and n_2 from using the gross count, net count, and peak ratio models above (Section 3.2) for the three scintillators. The standard deviation for the two datasets, s_1 and s_2, were determined as follows:

$$s_i = x_i\left(\frac{\sigma_{Ni}}{C_{Ni}}\right)$$

where C_{Ni} is the net total count arising from the 186 keV full-energy peak over duration n_i, and σ_{Ni} is the standard deviation of C_{Ni} determined using the errors associated with the respective linear regression model parameters, dM and dC.

This performance measurement replicates in-line production enrichment checks of single pellets, before and after sintering, and prior to loading into fuel pins. In this scenario there is a requirement to minimise the counting times of individual pellets so that as many as possible pellets within a batch are analysed to provide quality assurance across the entire batch in production. For this analysis, the tested null hypothesis was that both the pellets being analysed were 4.00 %wt enrichment. The results of this analysis, shown in Table 6, establish the time taken for the Behrens-Welch test statistic (*d*) to be greater than the alpha value for the chosen confidence level. At this counting duration, the difference in results suggests there is enough statistical confidence that the two values are sufficiently different as not to be the same enrichment.

From Tables 6 and it is evident that times required to distinguish between the two enrichments are very close across the detectors used for each method, e.g., for the net count method and a confidence level of 95%, 103, 141, and 124 s are required for the NaI(Tl), CsI(Tl) and SrI_2(Eu) respectively. This is expected given the similar earlier experimental results and χ_ν^2 values describing the goodness of fit for the models.

Nevertheless, the SrI_2(Eu) detector demonstrates the lowest required analysis times for the peak-ratio enrichment measurement method, and very close values to the NaI(Tl) for the gross and net count methods. The differences in duration for these two methods compared to the other two scintillators is small when using low confidence interval values but increases as the degree of confidence in the measurement increases. As can be seen in Table 6, the net-count method the SrI_2(Eu) detector reaches the required test statistic value, indicating a difference in enrichment, at 33 s for the 68% confidence interval, compared to 28 s for the NaI(Tl). When a 95% confidence limit is required, the difference increases to 21 s. This is a consequence of the relative size of the error in the results obtained by the SrI_2(Eu) compared to the other two scintillators, specifically the better net-to-gross count ratio.

It should be noted that the times in Table 6 refer to *real time*, rather than the detector *live time* operation mode used in the analysis in Section 3.2. As such, the times for the SrI_2(Eu) may increase marginally because of detector dead-time from the need for longer pulse shape timings. Using the percentage dead time of 0.76%, recorded using the SrI_2(Eu) for the 4.460 %wt pellet, this would equate to increasing the time for meeting the 95% confidence interval using the SrI_2(Eu) and net count method from 124 s to 125 s.

It should be reiterated, that the inclusion of the counts from the 163.3 and 205.1 keV emissions in the NaI(Tl) and CsI(Tl) detectors data increases the number of counts associated with the 186 keV line, making the detector appear more efficient and thus lowering the time required to differentiate the two enrichments for the detector. As discussed above, this is a recurring issue in both the efficiency comparison and the single pellet enrichment analysis. To alleviate this issue, different peak limits could be chosen to either include or exclude these emissions, by narrowing the energy window or expanding it for all the detectors or using a more sophisticated fit of the peak structure in this energy region. However, this would create additional statistical factors that would complicate the results unnecessarily, whereas the SrI_2(Eu) detectors are not affected by this issue.

4. Conclusion

This research shows that SrI_2(Eu) is a high-performing scintillation medium, relative to scintillation detectors in more widespread use, albeit available in larger sizes. The 43.1 cm^3 SrI_2(Eu) detector used in this research demonstrates superior energy resolution (3.43 ± 0.03% @ 662 keV) despite being substantially smaller in volume than the 347.5 cm^3 NaI(Tl) and 125 cm^3 CsI(Tl) also studied. The SrI_2(Eu) can identify the 163.3 and 205.1 keV peaks from ^{235}U, unlike the other two scintillators. The energy resolution for the SrI_2(Eu) reported here is in the middle of the range of resolutions described in other studies utilising SrI_2(Eu). This is likely because of the relative larger size of the SrI_2(Eu) crystal used here and the associated effects of self-absorption. The

Table 6
Limit of detection times (s) to differentiate 3.82% and 4.00% enriched AGR fuel pellets with a Behrens-Welch test approach, using the gross count-rate (G), net count-rate (N), and peak-ratio (PR) regression models in Fig. 6 for the NaI(Tl), CsI(Tl), and SrI2(Eu) scintillators and for four confidence intervals.

Scintillator		NaI(Tl)/s			CsI(Tl)/s			SrI_2(Eu)/s		
CI	#σ	G	N	PR	G (s)	N	PR	G	N	PR
68 %	1.00	31	28	49	36	38	56	34	33	45
90 %	1.65	80	72	128	94	99	146	89	87	117
95 %	1.96	114	103	183	134	141	209	126	124	166
99.5 %	2.58	200	181	322	236	248	364	222	219	294

resolution might be improved further by precise control of experimental geometries, collimated γ-ray beams, and the use of digital pulse processing to remove the documented light scattering inherent to large $SrI_2(Eu)$ crystals.

For its volume, the $SrI_2(Eu)$ demonstrates a high efficiency in the energy range used for the infinite thickness enrichment measurements of uranium (186 keV), as shown in the better net-to-gross count ratios. This is due to the relative volume inside the $SrI_2(Eu)$ scintillator subtended by the collimated γ-ray photons emitted from the pellets, compared to the larger NaI(Tl) and CsI(Tl) scintillators which have a higher likelihood of photons scattered off the collimator. The combination of excellent energy resolution and high efficiency places $SrI_2(Eu)$ amongst the best scintillators for use in radiological assays in the sub-250 keV energy range.

When applied to uranium enrichment measurements of AGR UO_2 fuel pellets, the $SrI_2(Eu)$ showed a comparable consistency compared to the more ubiquitous NaI(Tl) and CsI(Tl), observing the linear proportionality of the ^{235}U fraction and the detected 186 keV counts. It required the lowest counting times to distinguish between 3.82 %wt and 4.00 %wt pellets using peak ratio measurement fits and required only marginally longer counting times compared to the larger NaI(Tl) when utilising the gross count and net count methods. Nevertheless, given the excellent energy resolution and comparable enrichment measurement performance, $SrI_2(Eu)$ is an ideal scintillator for detailed passive γ-ray spectrometry of uranium-containing materials. Future research will explore the use of $SrI_2(Eu)$ scintillators in multi-probe UO_2 fuel pin measurements.

CRediT authorship contribution statement

Andrew J. Parker: Writing – review & editing, Writing – original draft, Methodology, Investigation, Formal analysis. **Manuel Bandala:** Writing – original draft. **Stephen Croft:** Writing – review & editing, Methodology. **Laurie Crouch:** Project administration, Data curation. **R. David Dunphy:** Writing – original draft, Investigation. **Daniel Hutchinson:** Writing – review & editing, Project administration, Investigation. **Roy Logsdon:** Resources. **Xiandong Ma:** Writing – review & editing, Supervision, Funding acquisition. **Stephen Marshall:** Writing – review & editing, Supervision, Funding acquisition. **Paul Murray:** Writing – review & editing, Supervision, Funding acquisition, Conceptualization. **Ali Sarfraz:** Investigation, Data curation. **Paul Stirzaker:** Project administration, Investigation. **James Taylor:** Supervision, Investigation, Funding acquisition. **Jaime Zabalza:** Writing – review & editing, Investigation, Formal analysis, Data curation. **Malcolm J. Joyce:** Writing – review & editing, Supervision, Investigation, Funding acquisition, Conceptualization.

Declaration of competing interest

The authors declare the following financial interests/personal relationships which may be considered as potential competing interests:

Malcolm Joyce reports financial support was provided by Engineering and Physical Sciences Research Council.

Data availability

The data that has been used is confidential.

Acknowledgements

This work was funded through a Engineering and Physical Sciences Research Council, United Kingdom grant EP/V051059. We would also like to acknowledge the contribution of the reviewers in improving the paper.

References

[1] T.C. Kaspar, C.A. Lavender, M.W. Dibert, Evaluation of Uranium-235 Measurement Techniques, 2017, https://doi.org/10.2172/1408200 [Online]. Available:.
[2] P. Bode, E.J. Hoffman, R.M. Lindstrom, S.J. Parry, R.J. Rosenberg, Practical Aspects of Operating a Neutron Activation, IAEA-TECDOC-564, Vienna, 1990.
[3] D. Reilly, N. Ensslin, H. Smith Jr., S. Kreiner, Passive Nondestructive Assay of Nuclear Materials, 1991.
[4] R. Mustonen, "Building Materials as Sources of Indoor Exposure to Ionizing Radiation," No. STUK-A105, Finnish Centre for Radiation and Nuclear Safety, 1992.
[5] N.J. Cherepy, et al., Strontium and barium iodide high light yield scintillators, Appl. Phys. Lett. 92 (8) (Feb. 2008) 83508, https://doi.org/10.1063/1.2885728.
[6] R. Hofstadter, Europium Activated Strontium Iodide Scintillators, 1968 3373279.
[7] F. Daghighian, et al., Evaluation of cerium doped lutetium oxyorthosilicate (LSO) scintillation crystal for PET, IEEE Trans. Nucl. Sci. 40 (4) (1993) 1045–1047, https://doi.org/10.1109/23.256710.
[8] F.L. Bronson, Initial performance testing of sri gamma spectroscopy scintillators and comparison to other improved-resolution detectors for typical health physics applications, EPJ Web Conf. 225 (2020) 09004, https://doi.org/10.1051/epjconf/202022509004.
[9] B.W. Sturm, et al., Evaluation of large volume SrI2(Eu) scintillator detectors, IEEE Nucl. Sci. Symp. Conf. Rec. 2 (2010) 1607–1611, https://doi.org/10.1109/NSSMIC.2010.5874047.
[10] M.S. Alekhin, J.T.M. De Haas, K.W. Kramer, I.V. Khodyuk, L. De Vries, P. Dorenbos, Scintillation properties and self absorption in SrI2:Eu 2, IEEE Nucl. Sci. Symp. Conf. Rec. (2010) 1589–1599, https://doi.org/10.1109/NSSMIC.2010.5874044.
[11] G.F. Knoll, Radiation Detection and Measurement, fourth ed., Wiley, New York, NY, 2010.
[12] R.N. Thomas, A. Paluszny, D. Hambley, F.M. Hawthorne, R.W. Zimmerman, Permeability of observed three dimensional fracture networks in spent fuel pins, J. Nucl. Mater. 510 (August) (2018) 613–622, https://doi.org/10.1016/j.jnucmat.2018.08.034.
[13] M. Takabe, A. Kishimoto, J. Kataoka, S. Sakuragi, Y. Yamasaki, Performance evaluation of newly developed SrI2(Eu) scintillator, Nucl. Instruments Methods Phys. Res. Sect. A Accel. Spectrometers, Detect. Assoc. Equip. 831 (2016) 260–264, https://doi.org/10.1016/j.nima.2016.04.043.
[14] P. Virtanen, et al., SciPy 1.0: fundamental algorithms for scientific computing in Python, Nat. Methods 17 (3) (2020) 261–272, https://doi.org/10.1038/s41592-019-0686-2.
[15] S.J. Fearn, S. Kaluvan, T.B. Scott, P.G. Martin, An open-source iterative Python module for the automated identification of photopeaks in photon spectra, Radiation 2 (2) (2022) 193–214, https://doi.org/10.3390/radiation2020014.
[16] Laboratoire National Henri Becquerel, Table de Radionucleides, 2010.
[17] P.R. Beck, et al., Strontium Iodide Instrument Development for Gamma Spectroscopy and Radioisotope Identification, 2014, https://doi.org/10.1117/12.2063056.
[18] Y. Wu, et al., Defect engineering in SrI2:Eu2+ single crystal scintillators, Cryst. Growth Des. 15 (8) (2015) 3929–3938, https://doi.org/10.1021/acs.cgd.5b00552.
[19] N.J. Cherepy, et al., SrI 2 scintillator for gamma ray spectroscopy, Spectrochim. Acta Part B At. Spectrosc. 7449 (2009), https://doi.org/10.1117/12.830016.
[20] A. Giaz, et al., Preliminary investigation of scintillator materials properties: SrI2: Eu, CeBr3 and GYGAG:Ce for gamma rays up to 9 MeV, Nucl. Instruments Methods Phys. Res. Sect. A Accel. Spectrometers, Detect. Assoc. Equip. 804 (2015) 212–220, https://doi.org/10.1016/j.nima.2015.09.065.
[21] Y.Y. Ji, H.S. Chang, T. Lim, W. Lee, Application of a SrI 2 (Eu) scintillation detector to in situ gamma-ray spectrometry in the environment, Radiat. Meas. 122 (January) (2019) 67–72, https://doi.org/10.1016/j.radmeas.2019.01.014.
[22] D.T. Vo, Comparison of portable detectors for uranium enrichment measurements, J. Radioanal. Nucl. Chem. 276 (3) (2008) 693–698, https://doi.org/10.1007/s10967-008-0619-5.
[23] Scionix, S1AB1467 - SrI2(Eu) Reference Datasheet, 2022.
[24] R. Hawrami, E. Ariesanti, V. Buliga, A. Burger, Thallium strontium iodide: a high efficiency scintillator for gamma-ray detection, Opt. Mater. 100 (2020) 7–12, https://doi.org/10.1016/j.optmat.2019.109624.
[25] M.C. Recker, E.J. Cazalas, J.W. McClory, J.E. Bevins, Comparison of SiPM and PMT performance using a Cs2LiYCl6:Ce3+ (CLYC) scintillator with two optical windows, IEEE Trans. Nucl. Sci. 66 (8) (2019) 1959–1965, https://doi.org/10.1109/TNS.2019.2926246.
[26] J. Rosado, Modeling the nonlinear response of silicon photomultipliers, IEEE Sensor. J. 19 (24) (2019) 12031–12039, https://doi.org/10.1109/JSEN.2019.2938018.
[27] L.J. Mitchell, B. Phlips, Characterization of strontium iodide scintillators with silicon photomultipliers, Nucl. Instruments Methods Phys. Res. Sect. A Accel. Spectrometers, Detect. Assoc. Equip. 820 (2016) (2016) 95–101, https://doi.org/10.1016/j.nima.2016.02.057.
[28] A. Raja, D. Joseph Daniel, P. Ramasamy, S.G. Singh, S. Sen, S.C. Gadkari, Difficulties and improvement in growth of Europium doped Strontium Iodide (SrI2: Eu2+) scintillator single crystal for radiation detection applications, J. Alloys Compd. 747 (2018) 989–993, https://doi.org/10.1016/j.jallcom.2018.03.097.
[29] I. Singh, B. Singh, B.S. Sandhu, A.D. Sabharwal, Comparative study for intermediate crystal size of NaI(Tl) scintillation detector, Rev. Sci. Instrum. 91 (7) (2020), https://doi.org/10.1063/5.0005243.
[30] M.S. Alekhin, J.T.M. De Haas, K.W. Kramer, P. Dorenbos, Scintillation properties of and self absorption in SrI2: Eu 2+, IEEE Trans. Nucl. Sci. 58 (5) (2011) 2519–2527, https://doi.org/10.1109/TNS.2011.2163642. PART 2.

[31] M. Moszyński, et al., Energy resolution of scintillation detectors, Nucl. Instruments Methods Phys. Res. Sect. A Accel. Spectrometers, Detect. Assoc. Equip. 805 (2016) 25–35, https://doi.org/10.1016/j.nima.2015.07.059.
[32] M. J. Berger et al., "XCOM: Photon Cross Sections Database." https://www.nist.gov/pml/xcom-photon-cross-sections-database (accessed November. 16, 2023).
[33] R. Berndt, E. Franke, P. Mortreau, 235U enrichment or UF6 mass determination on UF6 cylinders with non-destructive analysis methods, Nucl. Instruments Methods Phys. Res. Sect. A Accel. Spectrometers, Detect. Assoc. Equip. 612 (2) (2010) 309–319, https://doi.org/10.1016/j.nima.2009.10.060.
[34] R. Berndt, P. Mortreau, 235U enrichment determination on UF6 cylinders with CZT detectors, Nucl. Instruments Methods Phys. Res. Sect. A Accel. Spectrometers, Detect. Assoc. Equip. 886 (November 2017) (2018) 40–47, https://doi.org/10.1016/j.nima.2017.11.026.
[35] N. McFerran, et al., Gamma-ray spectrum variations for surface measurements of uranium hexafluoride cylinders, Nucl. Instruments Methods Phys. Res. Sect. A Accel. Spectrometers, Detect. Assoc. Equip. 961 (February) (2020) 163675, https://doi.org/10.1016/j.nima.2020.163675.
[36] H. Liu, et al., An approach to measure the enrichment of 235U by enrichment meter principle without knowing the thickness of intervening matter, Nucl. Instruments Methods Phys. Res. Sect. A Accel. Spectrometers, Detect. Assoc. Equip. 949 (August 2019) (2020) 162917, https://doi.org/10.1016/j.nima.2019.162917.
[37] N.C. Tam, J. Zsigrai, L. Lakosi, E. József, J. Sáfár, Non-destructive analysis of low-enriched and natural U samples by γ-spectrometry, Nucl. Instruments Methods Phys. Res. Sect. A Accel. Spectrometers, Detect. Assoc. Equip. 515 (3) (2003) 644–650, https://doi.org/10.1016/j.nima.2003.06.009.
[38] P.R. Bevington, D.K. Robinson, Data Reduction and Error Analysis for the Physical Sciences, third ed., McGraw-Hill Higher Education, New York, 2003.
[39] M. Tohamy, et al., Passive Non-Destructive Assay based on gamma-ray spectrometry to verify UO2 samples in the form of powder and pellet, Ann. Nucl. Energy 87 (P2) (2016) 186–191, https://doi.org/10.1016/j.anucene.2015.09.001.
[40] I. Meleshenkovskii, N. Pauly, P.E. Labeau, Determination of the uranium enrichment without calibration standards using a 500 mm 3 CdZnTe room temperature detector with a hybrid methodology based on peak ratios method and Monte Carlo counting efficiency simulations, Appl. Radiat. Isot. 148 (December 2018) (2019) 277–289, https://doi.org/10.1016/j.apradiso.2018.12.025.
[41] IAEA, "Advanced Methods of Process/quality Control in Nuclear Reactor Fuel Manufacture.".
[42] J.R. Nedelman, X. Jia, An extension of Satterthwaite's approximation applied to pharmacokinetics, J. Biopharm. Stat. 8 (2) (May 1998) 317–328, https://doi.org/10.1080/10543409808835241.
[43] T.K. Kim, T test as a parametric statistic, in: A. Potochnik, M. Colombo, C. Wright (Eds.), Statistics and Probability, Routledge, 2018, pp. 167–206.
[44] L.A. Currie, Limits for qualitative detection and quantitative determination. Application to radiochemistry, Anal. Chem. 40 (3) (1968) 586–593.